The Penn West CO_2 injection project: time-lapse monitoring with walkaway VSPs

Marcia L. Couëslan, Don C. Lawton and Michael Jones

ABSTRACT

At the Penn West CO_2 pilot project, 100 km southwest of Edmonton, Alberta, CO_2 is being injected into the Cardium Formation at a depth of 1620 m in the Pembina Oil Field for enhanced recovery and carbon sequestration purposes. The reservoir is being monitored using simultaneously acquired time-lapse multicomponent surface and borehole seismic surveys. Together, these provide lateral coverage of the survey area as well as high-resolution images near the observation well. The baseline survey was acquired in March 2005 prior to CO_2 injection. Both the P-wave and Sv-wave VSP images show excellent ties with the P-wave surface seismic data and have higher frequency bandwidth and resolution. The migrated images cover a 100 m radius of the reservoir around the observation well. The first monitor survey was acquired in December 2005 after eight months of CO_2 injection. Comparisons between the baseline and monitor borehole seismic surveys show an increase in reflectivity at the reservoir, and crosscorrelations show a time shift of 0.2 ms at the base of the reservoir on one of the walkaway lines. The baseline and monitor surveys also have nearly identical amplitude and phase spectra up to 80 Hz.

INTRODUCTION

Many of Western Canada's major oil and gas fields have been depleted through primary production and secondary recovery methods. Injecting CO_2 into a reservoir enhances oil recovery (EOR), reduces water usage, and has the potential benefit of CO_2 sequestration thereby reducing greenhouse gas emissions into the atmosphere. However, the injected CO_2 must be monitored to show that it is being trapped in these reservoirs and is not leaking back to the surface. Time-lapse surface seismic surveys have proved an effective tool in monitoring the injected CO_2 plume at the Weyburn CO_2 injection project (Davis et al., 2003) while time-lapse borehole seismic surveys were successfully used to monitor injected CO_2 at the Patrick Draw Field in Wyoming (O'Brien et al., 2004). In both of these cases, P- and Sv-wave amplitude and traveltime anomalies were used to identify the distribution of CO_2 in the reservoir.

At the Penn West pilot project, 100 km southwest of Edmonton, Alberta, CO_2 is being injected into the Cardium Formation in the Pembina Oil Field for enhanced recovery and carbon sequestration purposes. The injected CO_2 is being monitored using a sparse multicomponent surface seismic program coupled with a borehole seismic array. Together, these provide lateral coverage of the survey area as well as high-resolution images near the observation well. The baseline survey was acquired in March 2005 prior to CO_2 injection. The first monitor survey was acquired in December 2005 after eight months of CO_2 injection.

PROJECT BACKGROUND

The Cardium Formation is the main reservoir rock in the Pembina Oil Field. It is Cretaceous in age and consists of one conglomerate unit and three sandstone units with a total thickness of about 20 m at 1620 m depth. It is sandwiched by the thick marine shales of the Lea Park Formation (above) and the Blackstone Formation (below). The dominant fracture trend in this area is NE-SW. The Cardium Formation is a weak P-wave reflector and exploration in the area has historically been driven by geology rather than geophysics. The top and base of the reservoir appear as a weakly tuned event in seismic data.

Penn West Petroleum provided access to an old production well for use as a monitoring well. In February 2005, eight three-component geophones as well as six pressure and temperature sensors, and two fluid sampling ports were cemented into the well near reservoir depths. The geophones are located between 1497 and 1640 m depth with a 20 m vertical spacing; only one geophone is located in the reservoir itself. The monitoring program for the site is comprised of seismic surveys, geochemical sampling, and the pressure-temperature measurements.

The seismic program consists of two east-west source-receiver lines and one north-south (Figure 1). These three lines are 3 km long and provide a good distribution of source-receiver offsets at the injection pad. Two short north-south receiver lines were also added in order to provide a small area of 3D coverage for the surface seismic survey (Figure 1). For the baseline and monitor survey data acquisition, all lines had a receiver interval of 20 m, a source interval of 40 m, and a charge size of 2 kg at a depth of 15 m. All of the shots in the surface seismic program were recorded into this downhole array. CO_2 injection commenced a week after the baseline survey at a rate of approximately 35 tonnes/day. The first monitor survey was acquired in December 2005.

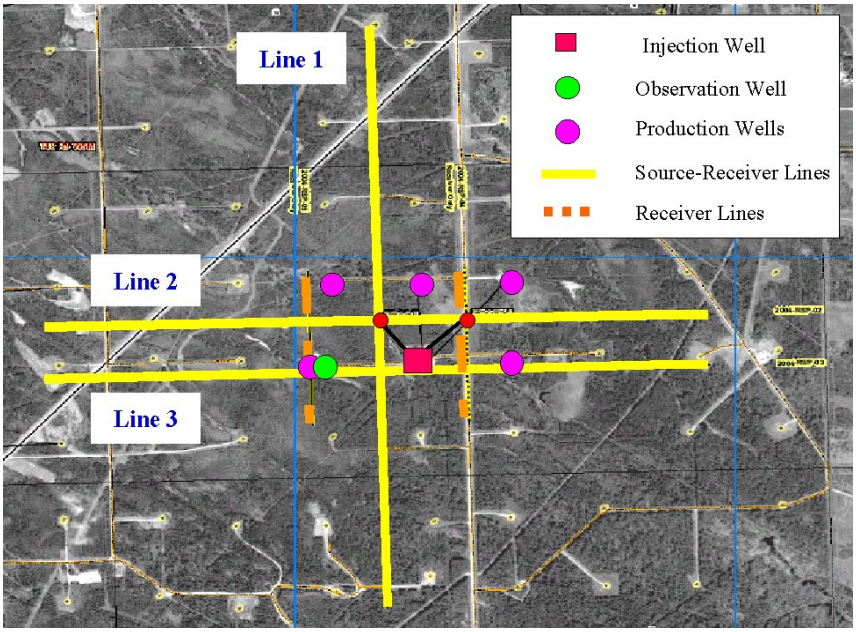

FIG. 1. Aerial view of the Violet Grove CO_2 Injection Site.

VSP PROCESSING

Data Rotations

When a VSP is acquired with a tool, or in this case a permanent receiver array, the geophones rotate as they are being raised or lowered into a well. As a result, the geophones in the array are not oriented in the same direction. In the case of a vertical well, this does not have a strong effect on the vertical component of the data, but it does have a strong effect on the horizontal components of the data. One of the horizontal components of data must be aligned in the direction of the maximum energy; in general, this is in the source-receiver plane for a particular shot. Hodogram analysis is used to determine the motion of the direct P-wave arrival within a small time window in the x, y, and z planes, and this information is used to orient the data to the source-receiver plane.

The hodograms from the raw x, y, and z components of the data demonstrated that the P-wave energy fell into distinct polarization planes (Figure 2). At the far offsets, the energy was evenly distributed between the vertical and horizontal components while the energy at the near offsets fell almost entirely in the vertical component. Ultimately, the raw data were rotated into the true earth frame (N, E, V) for the wavefield separation.

Anisotropic Velocity Model

An anisotropic velocity model was built both for the wavefield separation and migrations. The P- and S-wave sonic logs from a nearby production well were used as a starting point for the initial velocity model. The P-wave sonic was calibrated using the zero-offset VSP shot. Most of the receivers are located in the black shale of the Lea Park Formation, and the elastic properties of shale are known to be anisotropic (Hornby et al., 1994). It is possible to determine whether or not there is local anisotropy at the receivers

using the slowness and polarization measurements from each shot. If the local anisotropy parameters are established, they can be used to limit the values for anisotropy obtained in the anisotropic inversion and will improve the wavefield separation (Leaney, 2002)

The apparent slowness and polarization angles can be derived from the data using parametric inversion (Leaney and Emersoy, 1990). Each shot processed with parametric inversion yields a slowness component and a polarization measurement for the downgoing P-wave, upgoing P-wave, downgoing converted SV-wave, and upgoing converted SV-waves (Horne and Leaney, 2000). Slowness-polarization inversion as defined by Horne and Leaney (2000) can then be used to determine the anisotropy parameters at the receivers.

Figure 3a and b show crossplots of the slowness and polarization components for each of the four wavefields at receiver 4; the phase of the Sv-wavefield has been rotated by 90^{o} for the purposes of display. The data points were initially inverted for an isotropic model and a second time for an anisotropic model. From Figure 2b, it is clear that the anisotropic model fits the data points better than the isotropic model. The average values obtained for epsilon and delta at all of the receivers were 0.14 and 0.07 respectively. These values were used as a constraint when the velocity model was inverted for anisotropy. In the inversion, the values of the anisotropy parameters were allowed to increase linearly with depth. Time residuals after inversion were less than 3 ms (Figure 4).

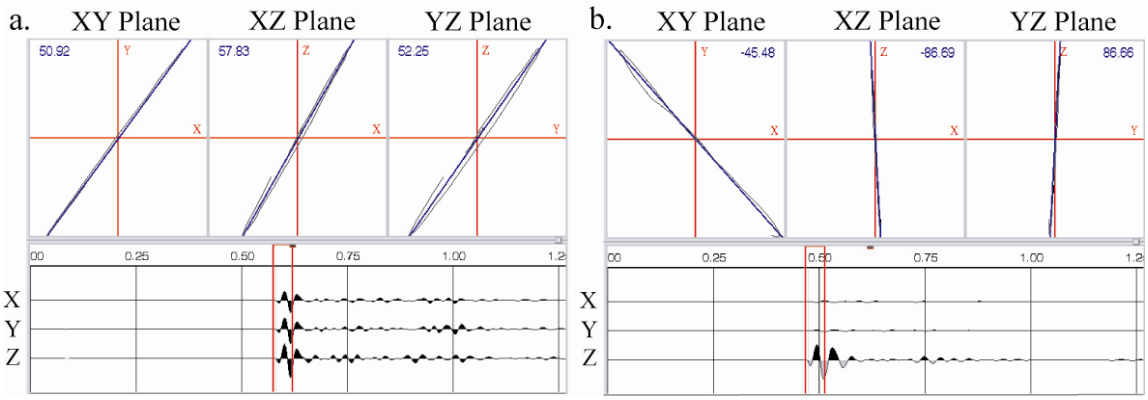

FIG. 2. (a.) Hodogram display from 1170 m west of the monitor well. (b.) Hodogram display from 10 m west of the well. At the far offset, the energy is evenly distributed between the x, y, and z planes. At 10 m offset, almost all of the energy is confined to the vertical component.

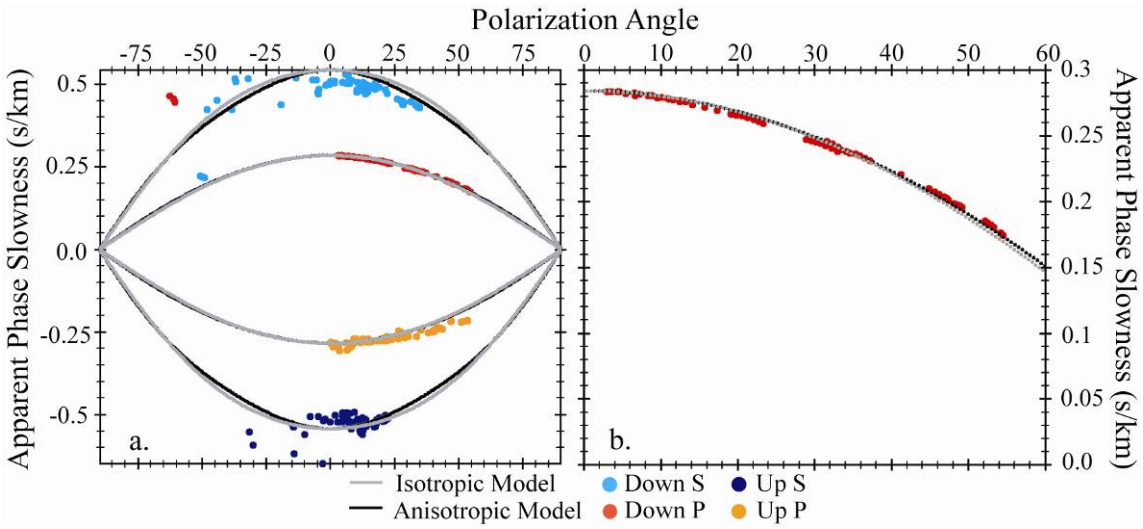

FIG. 3. Example of the anisotropy analysis using the slowness and polarization measurements derived from the parametric inversion at receiver 4. The data points tend to fall on the anisotropic model. (a) all of the data points. (b) detail of the downgoing P-wave data points.

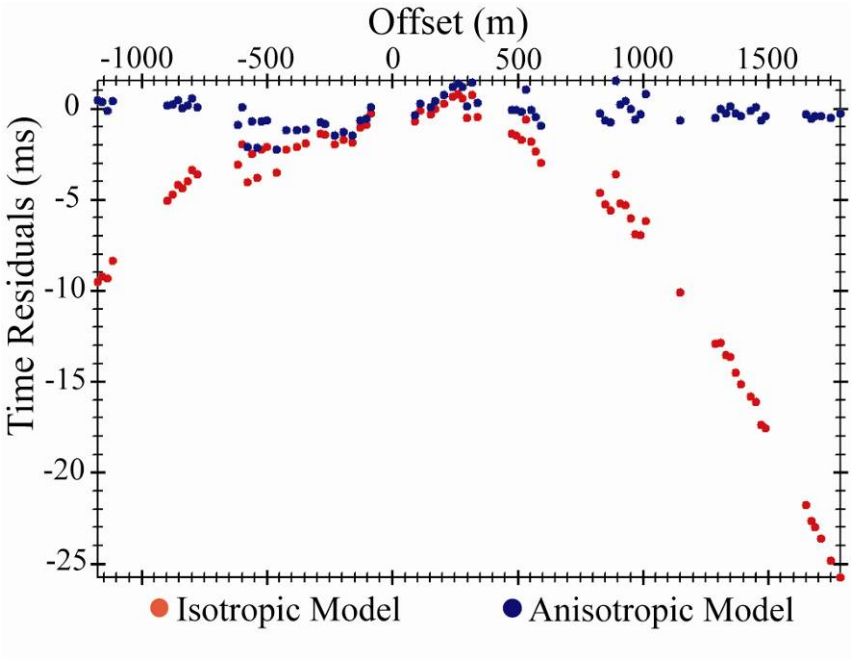

FIG. 4. Travel time residuals for the isotropic and anisotropic velocity models. After inversion for anisotropy, the residuals were less than 3 ms.

Wavefield Separation and Deconvolution

The wavefield separation method used is related to parametric wavefield decomposition as developed by Leaney and Esmersoy (1989). It is a least squares vector wavefield separation technique that separates the data into the following scalar wavefield components: down and upgoing P, down and upgoing Sv, and down and upgoing Sh. It has the following benefits over parametric inversion: it can separate the Sv- and Sh-wavefields, it deals with irregular source-receiver geometries, and it can incorporate

anisotropy into the wavefield separation. Figure 5 shows an example of the upgoing P- and Sv-wavefields from receiver 4 on the east-west line that runs closest to the monitor well (Line 3).

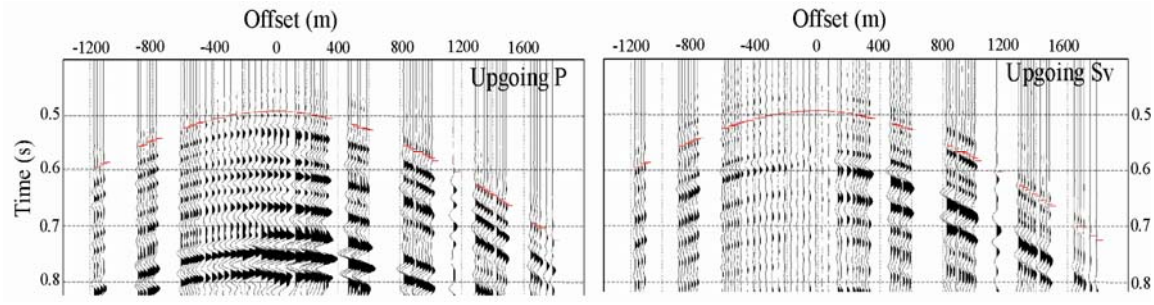

FIG. 5. The upgoing P- and Sv-wavefields from the wavefield separation from receiver 4, Line 3.

For this dataset, waveshaping deconvolution was used to restore the downgoing waveshape to its original form. The deconvolution operator attempts to collapse the direct downgoing wavefield to a single spike and removes the effect of that source signature from upgoing wavefields, thus matching the amplitude-frequency response of adjacent traces. The compressional wavefield was deconvolved using a frequency range from 8 to 100 Hz while the shear wavefield was deconvolved using a frequency range from 8 to 90 Hz. A window of 1.0 s and 1% whitening was used in the deconvolution process. The upgoing wavefields were normalized using the deconvolved downgoing P-wavefield.

Migration

The upgoing P- and Sv-wavefields from each survey were migrated with the anisotropic velocity model and a proprietary 1D VTI Kirchhoff migration algorithm. Figure 6 shows the comparison between images from the P-wave surface and borehole seismic data for Line 3. The VSP images show excellent ties to the surface seismic data as well as increased vertical and lateral resolution. The migrated P-wave VSP data clearly images the Cardium Formation for a radius of nearly 100 m around the observation well.

The Sv-wave data were migrated and converted directly into P-wave time so that it could be compared to the P-wave borehole seismic and surface seismic images. In Figure 7, the Sv-wave events can be clearly tied to events on the P-wave surface seismic. Some of the events on the Sv-wave image show more detail and higher resolution than the migrated P-wave VSP.

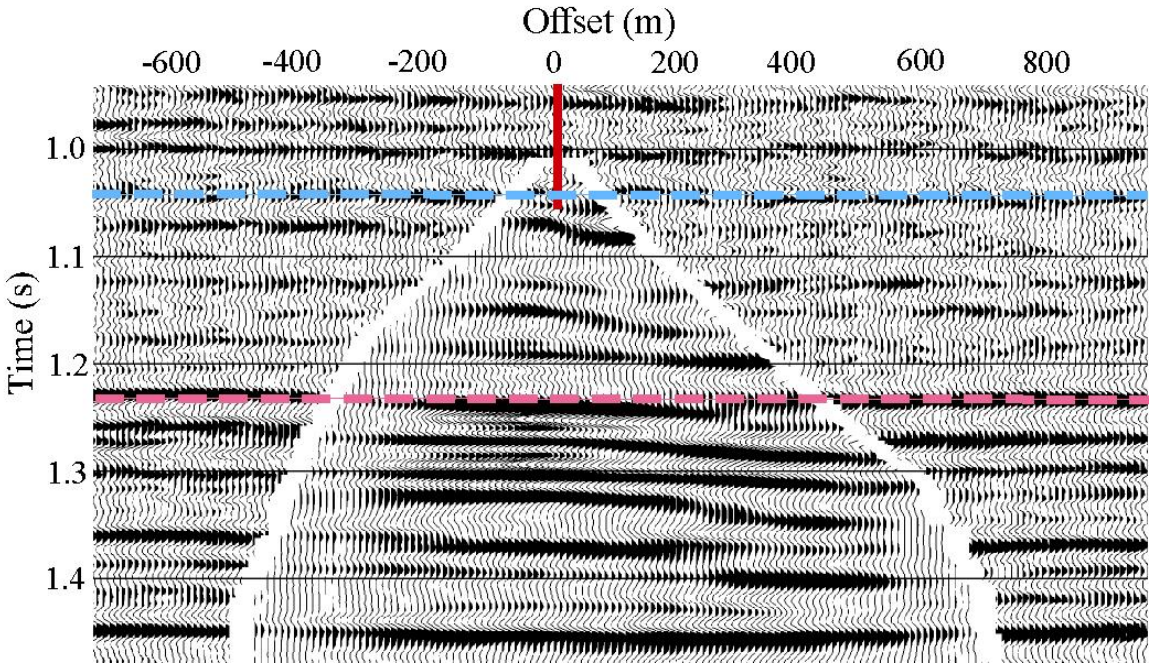

FIG. 6. Tie between the P-wave VSP and surface seismic data for Line 3. The Cardium Formation is in blue, the Viking Formation is in pink.

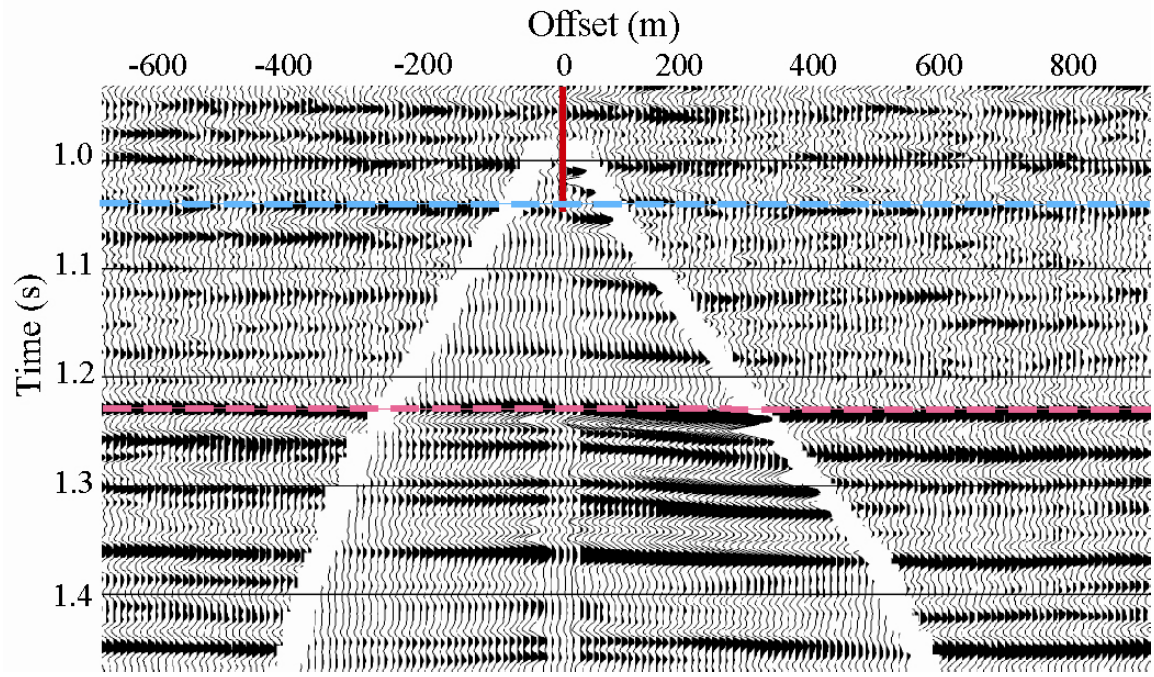

FIG. 7. Tie between the migrated Sv-wave VSP and the P-wave surface seismic from Line 3. The Cardium Formation is in blue, and the Viking Formation is in pink.

TIME-LAPSE RESULTS

Source Repeatability

The success of time-lapse seismic surveys depends strongly on repeating the acquisition parameters of the baseline survey in subsequent monitor surveys (Calvert, 2005). Shot locations that are removed or skidded in monitor surveys will result in differences that are not related to fluid substitution in the reservoir, and these differences may overwhelm the subtle amplitude and time shift differences caused by the injected CO_2.

For this project, two finite difference models were created using the source geometry from the baseline and monitor surveys and the anisotropic velocity model to demonstrate the effects of non-repeated shots on the difference displays. A total of 6 shots between the baseline and monitor surveys were not repeated. In Figures 8a and b, the two migrated synthetic datasets initially appear to be very similar. However, in Figure 8c, the difference display clearly shows the effect of the non-repeated shots.

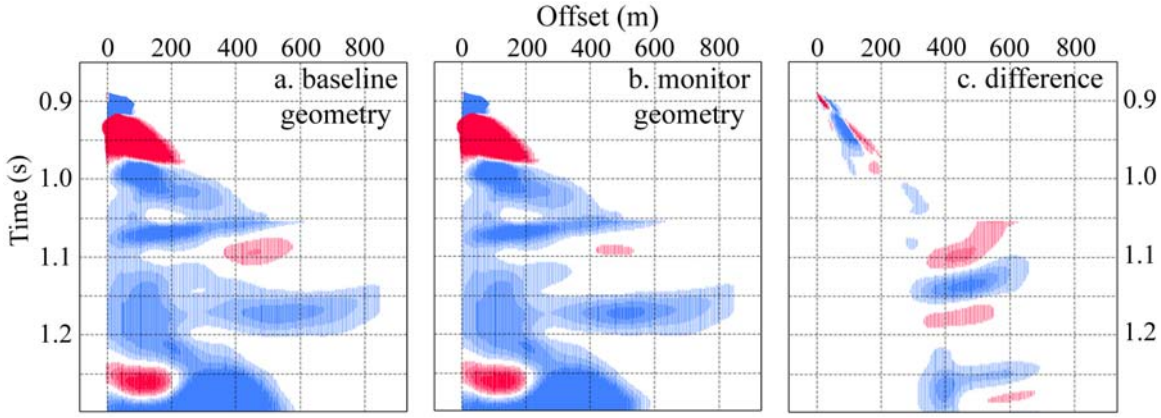

FIG. 8. (a) Migrated synthetic dataset using baseline source locations. (b) Migrated synthetic dataset with monitor source locations including 3 skidded shots. (c) The difference between the two synthetic datasets clearly shows the effect of non-repeated shots.

Initially, it was believed that all of the data should be used and that the migration would balance the amplitudes of the non-repeated shots (Figures 9a and b). Unfortunately, when the difference display was produced for Line 2, it was obvious that the skidded shots produced differences that were overwhelming the more subtle changes in the data (Figure 9c). When the non-repeated shots were removed from the baseline and monitor surveys prior to migration, the difference display started to show what are interpreted to be valid time-lapse changes (Figure 9d). In the final processing flow, all of the source locations that varied by more than 50 cm, or traces that were noisy in either of the surveys, were removed from the datasets so that they would not affect the time-lapse analysis.

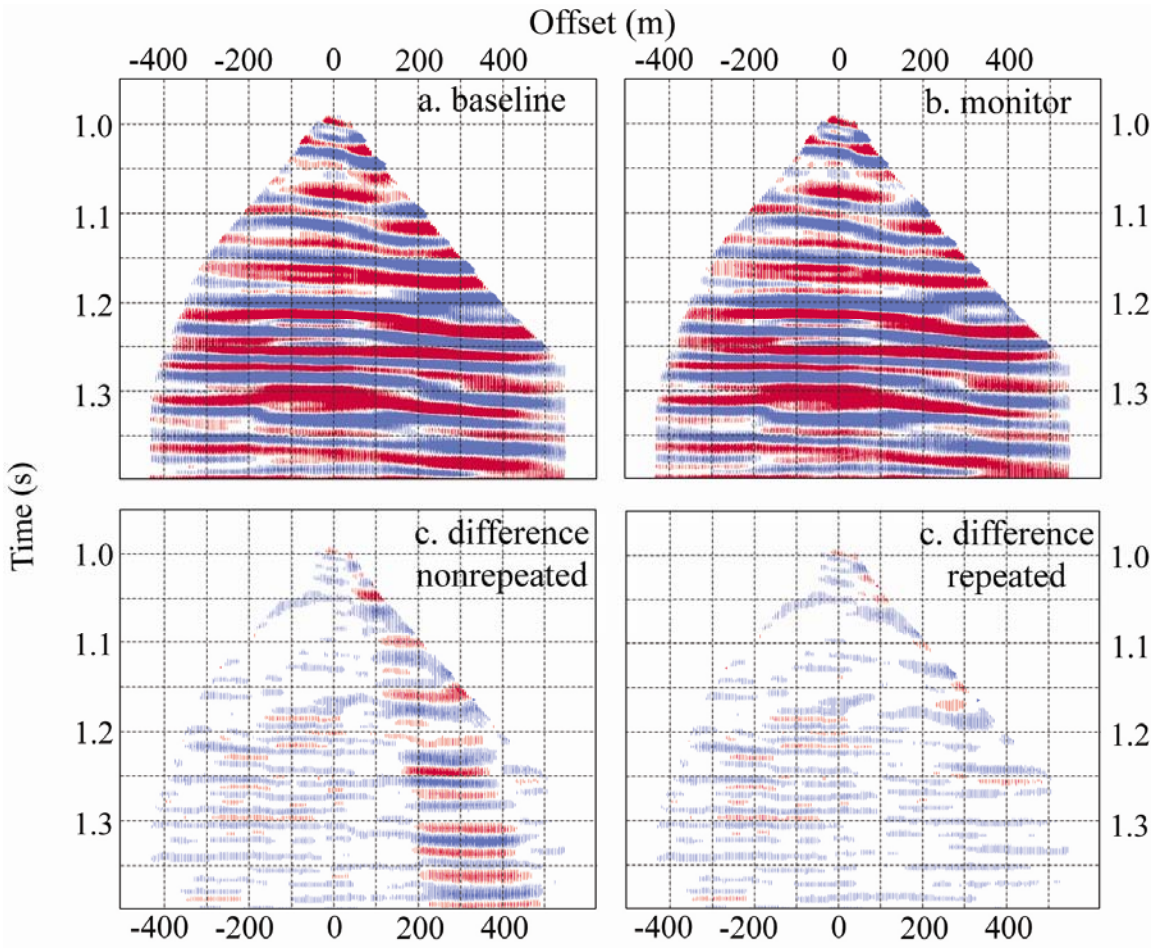

FIG. 9. The migrated P-wave VSP data containing all of the non-repeated shot locations for (a) baseline survey and (b) the monitor survey. (c) The difference display with the non-repeated shots. (d) The difference display with the non-repeated shots removed prior to migration.

Time Shifts Between Surveys

A bulk time shift of 3 ms was observed between the baseline and monitor survey (Figure 10). A similar time shift that extended to the surface was also observed in the surface seismic surveys, so the shift could not have been caused by the injected CO_2. Time shifts, caused by in the injected CO_2, should only occur at or below the depth of injection. The observed time shift could be caused by a number of factors such as differences in the near surface conditions. Prior to the wavefield separation, the difference in the baseline and monitor survey travel times for receiver 1 were used shift the monitor dataset to match the baseline dataset. Since receiver 1 lies well above the reservoir, and should be affected by the injected CO_2, this static shift is valid.

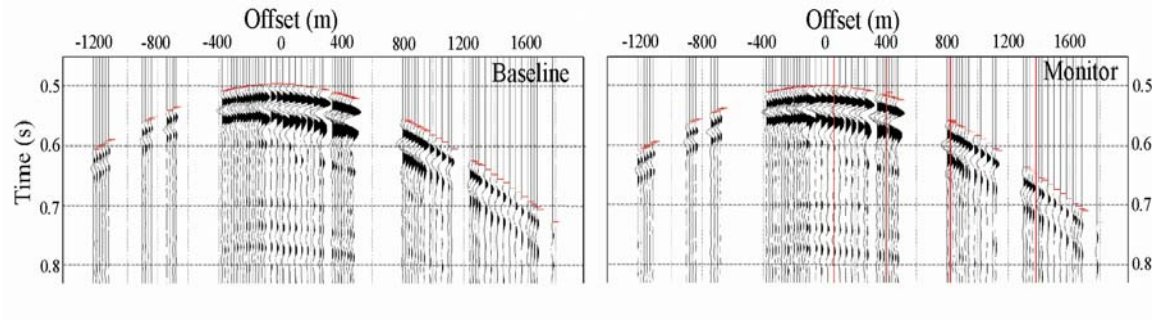

FIG. 10. Comparison of the raw data from receiver 4 on Line 2. The two datasets show a remarkable degree of similarity. The time shift between the two surveys is approximately 3 ms. The red lines in the Monitor display indicate non-repeated shots that have been removed from the dataset.

Difference Displays

The difference displays between the baseline and monitor surveys were examined for changes in the reservoir amplitudes, timing of events, and the amplitude and phase spectra. The P- and Sv-wave difference displays from Line 2 shows the clearest time-lapse differences (Figure 11). At the Cardium Formation event, the amplitudes have increased between the baseline and monitor surveys. An increase in amplitude that correlates directly to an actual seismic event has not been identified on later events. There appears to be a greater time shift in the Sv-wave data than in the P-wave data.

It is apparent there are other changes in the difference figures that are not related to the reservoir. A comparison of the amplitude and phase spectra of the two surveys shows that they are nearly identical at frequencies below 80 Hz without the use of a matching filter (Figure 12). However, these small differences in the amplitude and phase spectra result in some of the high frequency events observable on the difference displays. The datasets need to be cross-equalized to match the amplitude and phase spectra are remove the coherent noise.

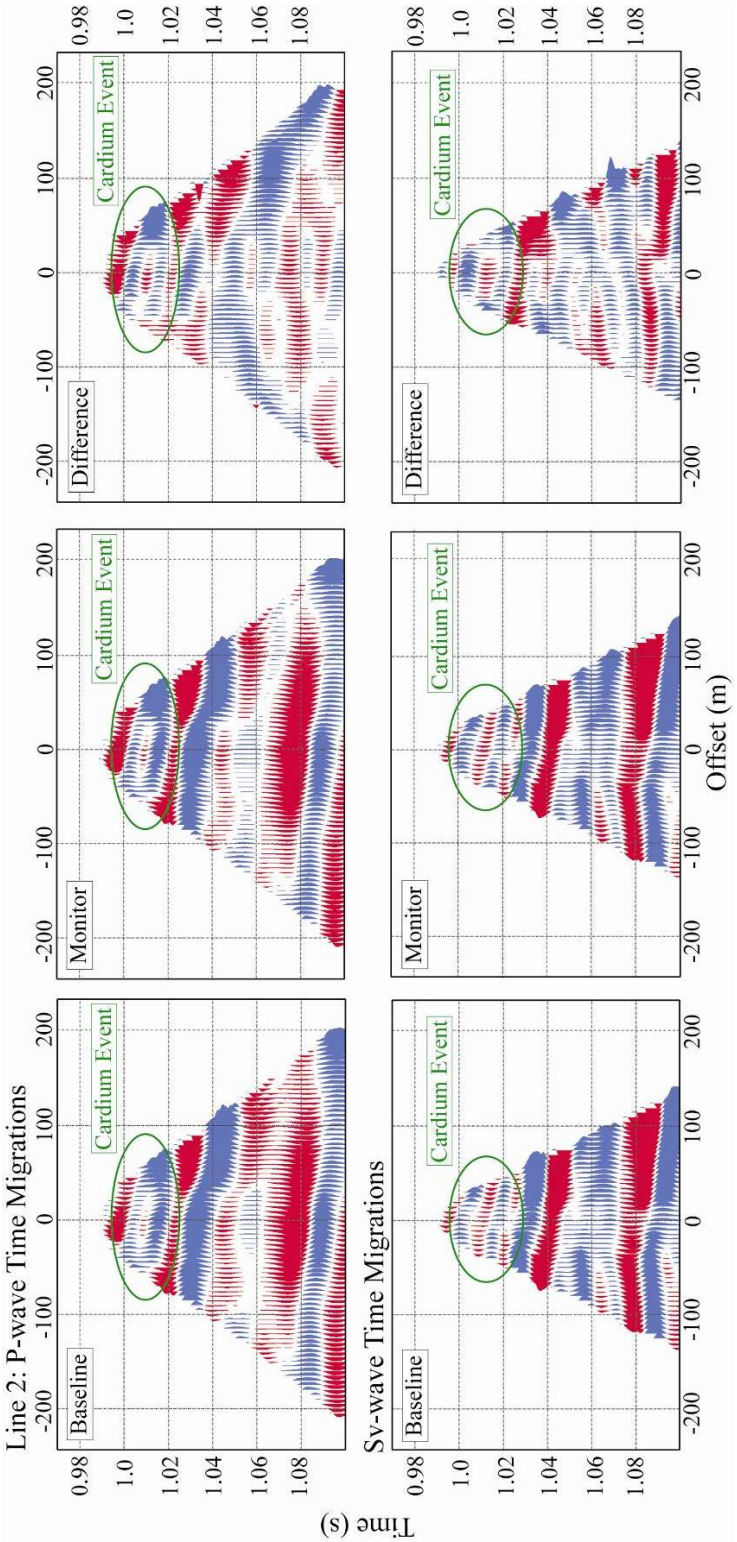

FIG. 11. Baseline and monitor survey time migrations and difference displays for the P- and Sv-wave data from Line 2. Amplitudes at the Cardium have increased up to 50% on some traces.

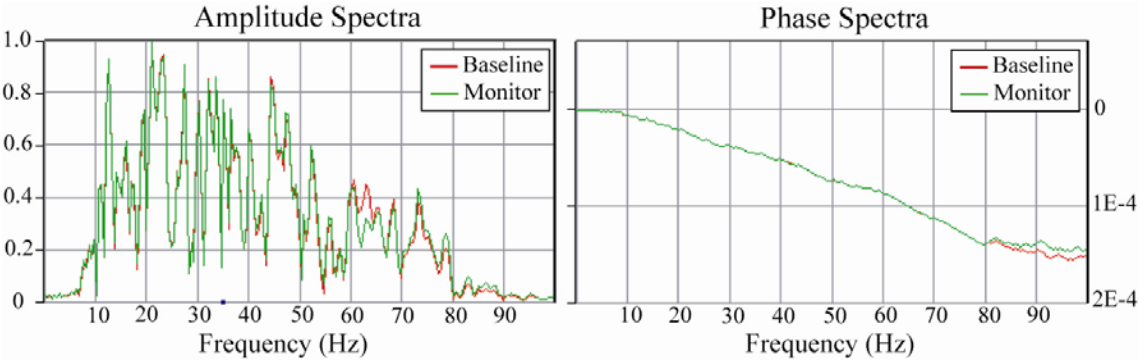

FIG. 12. The amplitude and phase spectra of the zero offset trace after migration from the baseline and monitor survey from Line 2. A matching filter has not been applied to either dataset. The spectra are nearly identical below 80 Hz.

Crosscorrelations

The baseline and monitor survey data were crosscorrelated in a 30 ms window around the base of the reservoir. The crosscorrelations displayed a systematic increase in travel time of 0.2 ms for the event. This is on the order of the time shift predicted with Gassman modeling, which indicates that a 10% saturation of CO_2 should cause a decrease in P-wave velocities of about 5% and result in time shifts of less than 1 ms (F. Chen, personal communication, 2006). Small time shifts for the base of the reservoir and deeper events are usually associated with fluid saturation changes and reservoir depletion. However, Landrø et al. (2005) and Meunier et al. (2000) have measured time shifts on the order of 0.2 ms related to small pressure variations in the reservoir.

The datasets were crosscorrelated in small windows around deeper events, and the time shift decreases with increasing depth. Below 1.4 s, no time shifts have been observed. A decrease in time shifts with depth has also been observed at the Weyburn CO_2 injection project (Li, 2003). This is probably due to the long offset shots undershooting the CO_2 plume. For long offset shots, the downgoing wave travels through the Cardium Formation well away from the observation well and beyond the CO_2 flood while the reflected wave passes through the CO_2 plume as it travels towards the geophones. As a result, the time shifts are too small to measure.

CONCLUSIONS

The P- and Sv-wave VSP images show excellent ties with the P-wave surface seismic data and have increased frequency bandwidth and resolution. The migrations image a disc about 200 m in diameter at the reservoir around the monitor well. The Sv-wave VSP image shows more detail and higher resolution on some events than the migrated P-wave VSP.

Crosscorrelations around the base of the reservoir of the baseline and monitor surveys from Line 2 show time shifts of 0.2 ms. This time shift is in the range of the shift predicted by the Gassmann equation modeling. The baseline and monitor surveys also have nearly identical amplitude and phase spectra up to 80 Hz. However, the small

differences that do exist result in high frequency events on the difference display. This can be corrected by cross-equalizing the data.

Results from the time-lapse analysis show an increase in the reflectivity of the reservoir on Line 2 in the eight months between the surveys. This indicates that the CO_2 flood is progressing southwest of the injector along the dominant fracture trend in the area. However, the main CO_2 front has not reached the monitor well or the nearby production well at this time.

The second monitor survey is due to be acquired in 2007. As the volume of CO_2 in the reservoir increases, it is expected that the reservoir reflectivity on Line 2 will continue to increase and that the CO_2 will begin to affect Lines 1 and 3 as well. The time shifts seen in the crosscorrelations should increase as the CO_2 displaces more of the oil.

ACKNOWLEDGEMENTS

We give special thanks to Scott Leaney with Schlumberger DCS in Houston, Texas for his advice on the wavefield separation, anisotropy analysis and velocity modeling, and migration. We also thank Schlumberger Canada for providing access to their resources to work on this project. Thanks also to Malcolm Bertram and Eric Gallant for their assistance with data acquisition.

The Penn West CO_2 monitoring project is funded through Alberta Energy Research Institute (AERI), Western Economic Diversification (WED), Natural Resources Canada (NRCan), grants from the Natural Sciences and Engineering Research Council of Canada (NSERC), Penn West Petroleum, and CREWES.

REFERENCES

Calvert, R., 2005, Insights and Methods for 4D Reservoir Monitoring and Characterization: 2005 Distinguished Instructor Short Course, Distinguished Instructor Series, No. 8

Davis, T.L., M.J. Martin, and R.D. Benson, 2003, Multicomponent seismic characterization and monitoring of the CO_2 Flood at Weyburn Field, Saskatchewan: The Leading Edge, **22**; 7: 696-697.

Hornby, B.E., L.M. Schwartz, and J.A. Hudson, 1994, Anisotropic effective-medium modeling of the elastic properties of shales: Geophysics, **59**; 10: 1570-1583.

Horne, S., and Leaney, S., 2000, Short Note: Polarization and slowness component inversion for TI anisotropy: Geophysical Prospecting, **48**, 779-788.

Landrø, M., P. Digranes, and L.K. Strønen, 2005, Pressure depletion measured by time-lapse VSP: The Leading Edge, **24**: 1226-1232.

Leaney, W. S. P., and Esmersoy, C., 1989, Parametric decomposition of offset VSP wave fields: 59th Ann. Internat. Mtg., Soc. Of Expl. Geophys., Expanded Abstracts, 1097-1100.

Leaney, W. S., 2002, Anisotropic vector plane wave decomposition of 3D VSP Data. 72th Ann. Internat. Mtg., Soc. Expl. Geophys., Expanded Abstracts, 2369-2372.

Li, G., 2003, 4D seismic monitoring of CO_2 flood in a thin fractured carbonate reservoir: The Leading Edge, **22**; 7: 690-695.

Meunier, J., F. Huguet, and P. Meynier, 2000, Reservoir Monitoring using Permanent Sources and Vertical Receiver Antennae: 70th Ann. Internat. Mtg., Soc. Of Expl. Geophys., Expanded Abstracts, 1619-1622.

O'Brien, J., F. Kilbride, and F. Lim, 2004, Time-lapse VSP reservoir monitoring. The Leading Edge, **23**; 11: 1178-1184.